Assessment of the Heat Transfer Model of a Helically Coiled Tube in MARS-KS and SPACE Codes

Tae Wook Ha[a], Jong-Hyuk Lee[a*]
[a] *Korea Atomic Energy Research Institute, 111, Daedeok-daero 989, Yuseong-gu, Daejeon, Republic of Korea*
[*] *Corresponding author: leejonghyuk@kaeri.re.kr*

Keywords : Heat transfer coefficient, Helically coiled tube, Nucleate boiling, Dryout

1. Introduction

The helically coiled heat exchangers are widely used because of their compact structure and higher heat transfer capability [1]. Due to these advantages, they have been used in a variety of fields, especially in air conditioning, nuclear systems, etc. In the field of nuclear system, many small modular reactors (SMRs), such as NuScale, SMART, i-SMR, etc., have adopted a helical coiled steam generator (HSG) due to its excellent heat transfer capability. Therefore, the accurate prediction of heat transfer in HSG is essential for the optimum design and safety analysis of these SMRs.

The heat transfer mechanism within a helical tube differ from that in a straight tube. In the thermal-hydraulic system codes, such as MARS and SPACE codes, the heat transfer model inside the tube of HSG is divided into the regions of single-phase liquid, nucleate boiling, transition boiling, and single-phase vapor. In this paper, a lot of experimental data have been collected for the heat transfer regions. Then, the heat transfer model inside the tube of HSG has been assessed against the experimental data in MARS-KS 2.0 and SPACE 3.3.2 codes. The results will be discussed in more detailed.

2. Heat transfer model of HSG

In this section, the heat transfer models of HSG for MARS-KS 2.0 and SPACE 3.3.2 codes are described. In addition, the PNU (Pusan National University) nucleate boiling model [2], recently implemented in the SPACE 3.3.2, is also described.

2.1 Description of HSG model

As mentioned earlier, in MARS-KS 2.0, and SPACE 3.3.2 codes, the heat transfer model inside the tube of HSG is divided into the regions of single-phase liquid, nucleate boiling, transition boiling, and single-phase vapor. The heat transfer models of both codes are almost the same for each region. For both codes, the single-phase liquid/vapor flow model [3] is presented as:

$$\ddot{q} = \hbar_{M-N}(T_w - T_f), \quad (1)$$

where, $\hbar_{M-N} = 0.03846\frac{k_f}{d}Re_f^{0.8} \times \frac{Pr_f}{\left(Pr_f^{2/3}-0.074\right)}\left(\frac{d}{D}\right)^{0.1}\left[1+\frac{0.098}{Re_f^{0.2}\left(\frac{d}{D}\right)^{0.4}}\right]$.

The Chen nucleate boing model [4] is represented as:

$$\ddot{q}_{NB} = h_{M-N}(T_w - T_f)F + h_{mic}(T_w - T_{sat})S, \quad (2)$$

where $h_{mic} = 0.00122\frac{k_l^{0.79}c_{p,l}^{0.45}\rho_l^{0.49}}{\sigma_l^{0.5}\mu_l^{0.29}h_{fg}^{0.24}\rho_v^{0.24}}(\Delta T_w)^{0.24} \times (\Delta p)^{0.75}S$.

In the MARS-KS code, the values of h_{M-N} and h_{mic} are respectively limited to a maximum of 50,000 W/m^{2}K. This is noted as a modification related to stability issue in the HSG for SMART reactor. On the other hand, there is no limit in the SPACE code.

For the transition boiling, the formation of chen correlation [5] is used as:

$$\ddot{q}_{TB} = \ddot{q}_{NB}a_f + \hbar_{M-N}(T_w - T_g)(1 - a_f), \quad (3)$$

where $a_f = 1.0 - \frac{\min[\alpha,0.999]-0.99}{0.009}$ for $\alpha \geq 0.99$.

For both codes, it is considered transition boiling, when the void fraction is greater than 0.99.

For $\alpha \geq 0.999$, Eq. (1) is used for the single-phase vapor region

In the MARS-KS and SPACE codes, the subcooled boiling model related to the void fraction consists of the net vapor generation (NVG) and the wall evaporation models. In the MARS-KS, the NVG and wall evaporation models are respectively follows:

- NVG model

$$h_{cr} = h_{f,sat} - \frac{1}{455}Nu'h_{fg} \text{ for Pe} \leq 70{,}000, \quad (4)$$

$$h_{cr} = h_{f,sat} - \frac{1}{0.0055 - 0.0009 \times F_{press}}\left(\frac{Nu'}{Pe}\right)h_{fg} \text{ for Pe} > 70{,}000, \quad (5)$$

where $Nu' = \frac{\ddot{q}D_hC_{pf}}{k_fh_{fg}}$.

- Wall evaporation model

$$\Gamma_w = \frac{q_w \cdot A_w}{V \cdot h_{fg}}\left(\frac{1}{1+\varepsilon_{SRL}}\right)\left[M + F_{press}(F_{gam} - M)\right], \quad (6)$$

where $M = \frac{h_f - h_{cr}}{h_f^S - h_{cr}}$,

$$F_{gam} = \min\left[1.0, 0.0022 + 0.11M - 0.59M^2 + 8.68M^3 - 11.29M^4 + 4.25M^5\right],$$

$$\varepsilon_{SRL} = \frac{\rho_f\left(h_f^S - h_f\right)\times F_{eps}}{\rho_g h_{fg}},$$

$$F_{eps} = min\left[1.0, \frac{1.0}{0.97+38exp\left[-\left(\frac{P}{6.894\times10^3}+60\right)/42\right]}\right],$$

$$F_{press} = \frac{1.0782}{1.015+exp\left[\left(\frac{P}{6.894\times10^3}-14\ .75\right)/28\right]}.$$

h_{cr} is the liquid enthalpy at the point of NVG and, Γ_w is the wall evaporation rate per unit volume. In the SPACE code, the NVG and wall evaporation models are respectively follows:

- NVG model

$$h_{cr} = h_{f,sat} - \frac{St' Pe^{0.124} C_{pf}}{0.0287} \text{ for Pe } \geq 52{,}000, \quad (7)$$

$$h_{cr} = h_{f,sat} - \frac{St' Pe^{1.08} C_{pf}}{918.525} \text{ for Pe } < 52{,}000, \quad (8)$$

where $St' = \frac{\ddot{q}}{GC_{pf}}$.

- Wall evaporation model

$$\Gamma_w = \frac{q_w \cdot A_w}{V \cdot h_{fg}}\left(\frac{1}{1+\varepsilon}\right) \times \left[M + \frac{1.0782\eta}{1.015+e^{\left[\left(\frac{P}{6.894\times10^3}-140.75\right)/28\right]}}\right], \quad (9)$$

where $M = \frac{h_f - h_{cr}}{h_f^S - h_{cr}}$,

$$\varepsilon = (1.51388K)F\frac{\rho_f}{\rho_g}\frac{C_{pf}(T_w - T_f)}{h_{fg}}\frac{\sqrt{k_f/\rho_f C_{pf} f}}{d_{Bw}}.$$

K is the bubble influence factor to be set as 4. The F factor is the inhibiting factor to satisfy the condition. A more detailed description is provided in Ref [6, 7].

2.2 Description of PNU nucleate boiling model

The PNU nucleate boiling model [2] has been developed for experimental data of saturated flow boiling in a helically coiled tube. The PNU model has been validated for a wide range of thermal-hydraulic conditions with pressures ranging from 1.0 to 140 bar, heat fluxes of 46 to 620 kW/m^2, mass fluxes of 77 to 1000kg/m^{2}s, D/d of 12.4 to 81.0. In the SPACE 3.3.2 code, the model has been implemented to replace the nucleate boiling model of Eq (2). The PNU nucleate boiling model is represented as:

$$\ddot{q}_{NB} = \hbar_{lo} C_1 Co^{C_2}\left(1 + C_3 N_{CF,l}\right)^{C_4}\left(T_w - T_f\right) + \hbar_{lo}(C_5 Bo^{C6} + C_7)(T_w - T_{sat}), \quad (4)$$

where, $\hbar_{lo} = 0.023 Re_f^{0.8} Pr_f^{0.4}\frac{k}{D}$,

$$Co = \left[\left(\frac{1-x}{x}\right)^{0.8}\left(\frac{\rho_g}{\rho_f}\right)^{0.5}\right], x = \frac{m_g}{m_{tot}},$$

$$N_{CF,l} = \frac{G^2(1-x)^2}{\alpha_l^2 \rho_l^2 g D_{HC}}\frac{2}{1+(P/\pi D_{HC})^2},$$

$$Bo = \frac{\ddot{q}}{G\hbar_{fg}},$$

$C_1 = 0.983$, $C_2 = -0.874$, $C_3 = 0.024$, $C_4 = 0.377$, $C_5 = 3858.4$, $C_6 = 0.920$, $C_7 = 0.517$.

3. Assessment of HSG heat transfer model

3.1 Experimental data

Some studies related to the HSG heat transfer have been conducted over several years. Among them, we have collected some experimental database to evaluate the HSG heat transfer model in both codes. As shown in Table 1, the experimental data covers a wide range of thermal-hydraulic conditions. The experimental data of Hardik and Prabhu [8] include the single-phase and nucleate boiling region (low quality region). The experimental data of Chang et al. [9] and Santini et al. [10] cover the nucleate boiling region (low- and high-quality region). The experimental data of Xiao et al. [11] include the transition boiling region (after dryout point). The experimental data of Wu et al. [12] include all flow regions.

Table 1. Experimental conditions

Experiment	Press. (bar)	Heat flux (kW/m^2)	Mass flux (kg/m^{2}s)	D/d (-)
Hardik and Prabhu [8]	1.0 ~2.0	100~620	129 ~400	14.4 17.1
Chang et al. [9]	80.0~ 110.0	100~290	500 ~1000	81.3
Santini et al. [10]	20.0 ~60.0	51~200	200 ~820	80.1
Xiao et al. [11]	20.0 ~48.0	200~400	400 ~800	12.4 30.4
Wu et al. [12]	24.0	250	250	247
Total	1.1 ~110	51~620	129 ~1000	12.4~ 247

3.2 Assessment results

The nodalization for the validation of heat transfer model of HSG is shown in Fig. 1. It consists of two boundary condition (TFBC), two pipes at the inlet and outlet of the heated section, and a pipe and a heat structure for the heated section of a helical tube. The heated section is divided into 20 nodes for each experiment.

Using the nodalization, the MARS-KS 2.0 and the SPACE 3.3.2 codes have assessed against the collected experimental data in Table 1. Figures 2(a) through (e) show representative simulation results for the collected experimental cases. The results show the following key findings.

As shown in Fig. 2(a), the simulation results of the MARS-KS 2.0 and SPACE 3.3.2 codes are considerably different, although the heat transfer model of the two codes are almost the same. The different results are because the void fraction calculated in the two codes are different and, therefore, the onset of transition boiling, so called first dryout point, is predicted differently. As shown in Figs. 2(a), (c), (d), (e), the MARS-KS code showed a tendency to predict the first dryout point earlier, compared to the SPACE code.

As shown in Figs. 2(c), (d), some experimental data show the values of HTC greater than 50,000 W/m^{2}K. For this experiment, the MARS-KS quite underpredicts the experimental data due to the limitation, as explained earlier.

From the simulation results, the MARS-KS 2.0 and the SPACE 3.3.2 codes mostly over-predicted the experimental data. For some simulation results of the MARS-KS code, the first dryout point ($\alpha \geq 0.99$) was predicted earlier and, thus, the MARS-KS code under-predicted the experimental data. The SPACE3.3.2_PNU, which uses the PNU nucleate boiling model instead of the Chen nucleate boiling model, mostly tended to underpredict the experimental data, but overall it showed the best agreement with experimental data among the three codes. As presented in Table 2, the RMSE assessment results also showed the best agreement of the SPACE3.3.2_PNU code.

As represented in Figs. 2(d), (e), It was also shown that, from the transition boiling region, the predictability of heat transfer coefficient considerably depends on the first dryout model (currently using $\alpha \geq 0.99$).

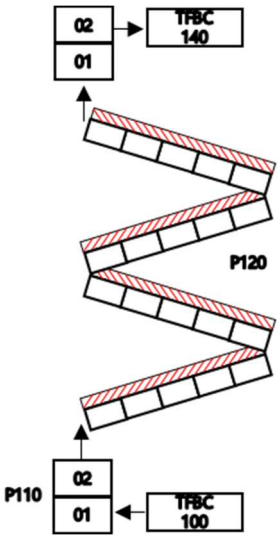

Fig. 1. The nodalization for the validation of heat transfer model of HSG.

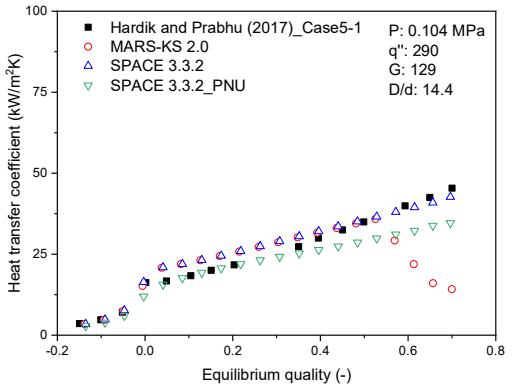

(a) Hardik and Prabhu

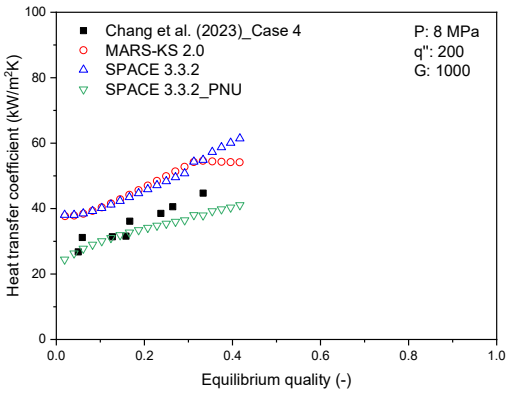

(b) Chang et al.

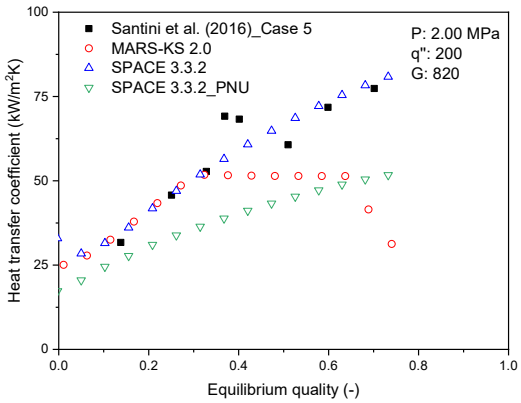

(c) Santini et al.

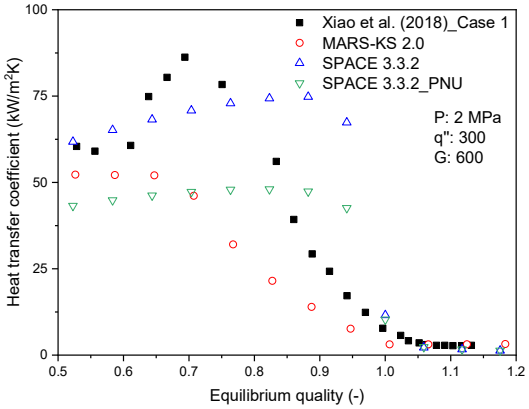

(d) Xiao et al.

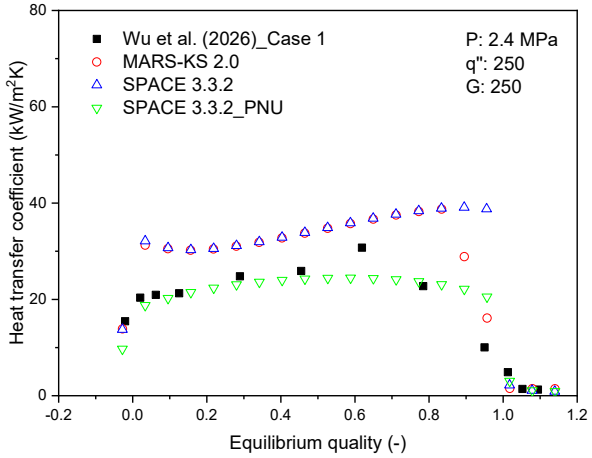

(e) Wu et al.

Fig. 2. The simulation results of the MARS-KS 1.6 and SPACE 3.3.2 codes.

Table 1. RMSE assessment results

Experiment	RMSE= $\sqrt{\frac{1}{N}\sum_{i=1}^{N}\left[\frac{\lvert h_{exp,i}-h_{cal,i}\rvert}{h_{exp,i}}\right]^2}$		
	MARS	SPACE	SPACE_PNU
Hardik and Prabhu [8]	0.21	0.17	0.21
Chang et al. [9]	0.23	0.23	0.30
Santini et al. [10]	0.37	0.35	0.29
Xiao et al. [11]	0.87	1.68	0.82
Wu et al. [12]	0.41	0.89	0.35
Total	0.42	0.67	0.39

4. Conclusions

In the MARS-KS 2.0 and SPACE 3.3.2 codes, the heat transfer coefficient model of a helically coiled tube has been assessed against experimental data. The results showed that the MARS-KS code predicts the first dryout point early and underpredicts some experimental data due to the limitation of heat transfer coefficient for the nucleate boiling region. The SPACE 3.3.2 mostly over-predicted the experimental data and, on the other hand, the SPACE 3.3.2_PNU underpredicted the experimental data. But overall the results of SPACE 3.3.2_PNU showed the best agreement with experimental data among the three calculation results. Furthermore, the predictability of heat transfer coefficient considerably depends on the first dryout model. Further studies are needed in this regard.

Acknowledgements

This work was supported by the Innovative Small Modular Reactor Development Agency grant funded by the Korea Government(MSIT) (No. RS-2024-00403548).

REFERENCES

[1] D. G. Prabhanjan, T. J. Rennie, G. S. V. Raghavan, Natural convection heat transfer from helical coiled tubes, Int. J. Therm. Sci., 43, 359, 2004.
[2] J.J. Jeong, T.G. Lee, S.G. Nam, B. Yun, Incorporating the effect of Centrifugal Force into the Correlation for Saturated Flow Boiling Heat Transfer in a Helically Coiled Tube, Nuclear Technology, 1-8, 2024.
[3] Y. Mori, W. Nakayama, Study on Forced Convective Heat Transfer in curved pipes, International Journal of Heat and Mass Transfer, 7, 1964.
[4] J. C. Chen, Correlation for boiling heat transfer to saturated fluids in convective flow, ASME, paper 63-HT-34, 1-11, 1963.
[5] J. C. Chen, R. K. Sundaram, F. T. Ozkaynak, Phenomenological correlation for post-CHF heat transfer, Lehigh University, Bethlehem, Pa (USA), Department of Mechanical Engineering and Mechanics, 1977.
[6] T.W. Ha, B.J. Yun, J.J. Jeong, Improvement of the subcooled boiling model for thermal-hydraulic system codes, Nuclear Engineering and Design, 364, 110641, 2020.
[7] K.S. Ha, Y.B. Lee, H.C. No, Improvements in predicting void fraction in subcooled boiling, Nuclear technology, 150(3), 283-292, 2005.
[8] B.K. Hardik and, S.V. Prabhu, Boiling pressure drop and local heat transfer distribution of helical coils with water at low pressure, International Journal of Thermal Sciences 114, 44-63, 2017.
[9] F.C. Chang, Y. Liu, J. Lou, Y. Shang, H. Hu, H. Li, Experimental investigation on flow boiling heat transfer characteristics of water and circumferential wall temperature inhomogeneity in a helically coiled tube, Chemical Engineering Science 272, 118592, 2023.
[10] L. Santini, A. Cioncolini, M. T. Butel, M. E. Ricotti, Flow boiling heat transfer in a helically coiled steam generator for nuclear power applications, International Journal of Heat and Mass Transfer 92, 91-99, 2016.
[11] Y. Xiao, Z. Hu, S. Chen, H. GU, Experimental investigation and prediction of post-dryout heat transfer for steam-water flow in helical coils, International Journal of Heat and Mass Transfer 127, 515-525, 2018.
[12] Z. Wu, Y. Shi, K. Li, K. Zhang, W. Tian, S. Qiu, Experimental study on boiling heat transfer characteristics in helical coils with large coiled diameters, Annals of Nuclear Energy, 225, 111793, 2026.